

A 3D FEM of Internal Gravity Waves

W.E.H.Sollie

27th February 2001

Contents

1	Introduction	2
2	Mathematical model	2
2.1	Introduction	2
2.2	Model equations	3
2.3	Properties of internal waves	5
2.4	Known solutions	8
2.5	Warp	10
3	Analytical methods	13
3.1	Introduction	13
3.2	Reflection expressions	13
3.3	Raytrace	15
4	Numerical methods	19
4.1	Introduction	19
4.2	FEM theory	21
4.3	FEM implementations	27
5	Numerical results	27
5.1	Introduction	27
5.2	Internal gravity waves	27
5.3	Inertial waves	29
6	Conclusions Summary	29

1 Introduction

When internal waves are present in a container, very interesting behavior can occur. For example when the container has a broken symmetry, so called attractors are possible. Of the full three dimensional solutions however, not very much is known. The subject of this report is the behavior of the internal waves in three dimensional geometry's. Because analytical methods fail in three dimensions for all but the most simple geometry's, one has to resort to numerical computation. This has been done in the past, Henderson & Aldridge (1992) made a finite element model (FEM) for internal waves in a frustum. The work done here has been based on a FEM made by A.N.Swart. This model was developed for examining the behavior of internal waves in a two dimensional way, where a constant pressure distribution in one direction is assumed. This FEM is based on the equations which describe the behavior of the internal waves in terms of the pressure alone. The FEM was implemented in MATLAB and has been used as a basis for the work done here. The research goal of this project was to extend the FEM code written by A.N.Swart to three dimensions. Using this code the three dimensional behavior of internal waves, in a special trapezoidal shaped container, had to be examined. So far the FEM model has been extended to three dimensions. Several versions were made, both for internal gravity waves and inertial waves. Also, by assuming a pressure distribution in one direction, some two dimensional simplifications of the three dimensional model were made and programmed. These codes have been tested and should be computationally correct. For the internal gravity waves, the code was checked by looking at the results in a cube, which can be derived analytically. For inertial waves, the code was checked with work done by L.Maas on the amphidromic structures of inertial waves in a cube. Analytically, some work was done by tracking the energy of the internal waves through the containers.

In chapter 2 the mathematical model describing the behavior of internal waves in a container is derived. Also some important properties of internal waves are presented. After this the known solutions are briefly discussed. Finally some features of the computer program warp are discussed. In chapter 3 some analytic work is presented, which mainly deals with tracking the energy through the three dimensional container, which gives an idea of the behavior. Using this analytic work the solutions for the cube and the expectations for the trapezoid are discussed. In chapter 4 the FEM extensions are described both in theory and implementation. Chapter 5 deals with the results of the FEM implementation(s). The results are presented and where possible explained and compared with known solutions. Finally, in chapter 6 the results are summarized.

2 Mathematical model

2.1 Introduction

In this chapter the mathematical model describing the behavior of internal waves in a closed container is set up. The mathematical model is derived in section 2.2.

This will result in a differential equation with boundary conditions in terms of the pressure. In this section some properties of the differential equation are also discussed. In section 2.3 internal waves are examined. Some important properties of internal waves, including the dispersion relation, energy propagation and reflection behavior, are described. In section 2.4 the known solutions are presented. Finally, in section 2.5 the finite element model Warp is presented.

2.2 Model equations

The behavior of internal waves in a rotating container is described by the linearised bousinesq equations :

$$\rho^*(\mathbf{u}_t + \mathbf{f} \times \mathbf{u}) = -\nabla p + \rho g \mathbf{k} \quad (1)$$

$$\rho_t - \frac{w \rho^* N^2}{g} = 0 \quad (2)$$

$$\nabla \cdot \mathbf{u} = 0 \quad (3)$$

The first equation is a linearised version of the euler equation for a rotating fluid. The second equation expresses that there is no compression or diffusion. The last equation is the continuity equation. A subscript indicates a derivative, while a bold typed variable indicates a vector. In these formulas p stands for the pressure perturbation, where the static part of the pressure is given by $\frac{dp_0}{dz} = -\rho_0 g$. N is the Brunt-Väisälä frequency, defined by : $N^2(z) = -\frac{g}{\rho^*} \left(\frac{d\rho_0}{dz} + \frac{\rho_0 g}{c_s^2} \right)$. The Brunt-Väisälä frequency will be assumed to be a constant. This means that the static part of the density is given by $\rho_0 = C e^{-z \frac{N^2 c_s^2 + g^2}{g c_s^2}}$, where $C \geq 0$ is arbitrary constant. Because the density of the water increases with depth the stratification is stable. ρ^* is the depth average of ρ_0 . $\mathbf{f} = (0, 0, f)$ is a vector containing the angular velocity $f/2$. It's direction is assumed to be in the positive z-direction, which is opposite to the direction of gravity. Because it is assumed that Boussinesq approximation holds, the description is valid for short wavelengths ($k^2 \gg N/g$). The linearisation is valid when the particle velocity is smaller than the phase velocity, which in turn should be smaller than the velocity of the surface waves ($|\mathbf{u}| \ll c \ll c_{surf}$). The effects of compressibility on the velocity are neglected. This assumption is valid when the phase velocity of the internal waves and the surface waves are much smaller than the speed of sound ($c \ll c_s$ and $c_{surf} \ll c_s$).

The particle velocity is now directly dependent on the pressure. By assuming a time dependence of $e^{-i\omega t}$, rewriting the first equation one finds :

$$u = \frac{i\omega p_x + f p_y}{\rho^*(\omega^2 - f^2)} \quad (4)$$

$$v = \frac{i\omega p_y - f p_x}{\rho^*(\omega^2 - f^2)} \quad (5)$$

$$w = \frac{i\omega p_z}{\rho^*(\omega^2 - N^2)} \quad (6)$$

By combining these expressions with the continuity equation, a differential equation is found in which the behavior of internal waves is described in terms

of the pressure alone : $p_{xx} + p_{yy} - \lambda p_{zz} = 0$, where $\lambda = \frac{\omega^2 - f^2}{N^2 - \omega^2}$. At the boundary of the container it is assumed that the flow is parallel to the boundary, so that there is no flow through the boundary. This condition, $\mathbf{u} \cdot \hat{\mathbf{n}} = 0$, combined with the expressions for the particle velocity give the boundary condition in terms of the pressure : $(p_x, p_y, -\lambda p_z) \cdot \hat{\mathbf{n}} = -\frac{f}{i\omega}(p_y, -p_x, 0) \cdot \hat{\mathbf{n}}$.

So the behavior of internal waves in a rotating container can be described in terms of the pressure alone :

$$p_{xx} + p_{yy} - \lambda p_{zz} = 0 \text{ on } V \quad (7)$$

$$(p_x, p_y, -\lambda p_z) \cdot \hat{\mathbf{n}} = -\frac{1}{i\omega}(\nabla p \times \mathbf{f}) \cdot \hat{\mathbf{n}} \text{ on } \delta V \quad (8)$$

ω is the frequency of the internal waves, which are assumed to be monochromatic, since a time dependence of $e^{-i\omega t}$ is assumed. V and δV are the interior and the boundary of the container. $\hat{\mathbf{n}}$ is the unity vector normal to the boundary δV , of which the direction depends on the place at the boundary.

When there is a stratification, N acts as an upper and f as a lower bound for the internal wave frequencies, and when there is no stratification f acts as an upper bound for the internal wave frequencies. In both these cases, so if $f^2 < \omega^2 < N^2$ or if $\omega^2 < f^2$, $\lambda > 0$ and the differential equation is hyperbolic in the z direction of the space. In all the other cases the differential equation is elliptic. When it's hyperbolic it's characteristic surfaces are then given by : $z = \pm(\lambda(x^2 + y^2))^{1/2} + C$. These surfaces can be seen as the top and bottom halves of a cone with center point $(0, 0, C)$ and with a radial slope of $\pm(\lambda)^{1/2}$. This is illustrated in figure 2, where the characteristics of the differential equation have the shape of the inner cone. Because the differential equation is hyperbolic, the solutions may be discontinuous along the characteristic surfaces. Also, the solutions are strongly dependent on the (local) shape of the characteristic surfaces and the boundary. The problem is for this reason called ill-posed, because minimal changes in the boundary can strongly influence the solutions.

In principle, the finite element method allows for arbitrary containers. In this project, one two different types of containers are used. The first container is the cube, which is used as a test case. The second geometry is the trapezoid (illustrated in figure 1), which is of interest because it has a broken symmetry and also because some experiments were done using this geometry. For the simulations a cube with sides of length 1, and a trapezoid of length, width and height of 1 and an offset of 1/2 was used.

By assuming a plane wave solution in the y -direction, a simplification can be made that causes the resulting problem to be of dimension two instead of dimension three. Taking a plane wave in the y -direction means that a pressure distribution of $p = p(x, z)e^{i(k_2 y - \omega t)}$ is assumed. To satisfy the boundary conditions the real part, $\text{Re}(p)$, of this solution has to be taken. One can interpret this as looking at a canal of infinite length in the y -direction, where internal waves are invoked in a linewise manner in the y -direction, so independent of the y -position. All the contributions to the solution in the y -direction are canceled out, which leaves a solution that only depends on the x and z positions. All possible directions (in the xy plane) of the waverays are still present, but there

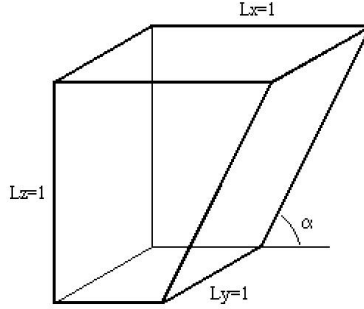


Figure 1: The trapezoid

is only one possible wavenumber for each direction. Putting this expression in the differential equation gives :

$$p_{xx} - \lambda p_{zz} - k_2^2 p = 0 \text{ on } V \quad (9)$$

$$(p_x, 0, -\lambda p_z) \cdot \hat{\mathbf{n}} = -\frac{fk_2}{\omega} (p, 0, 0) \cdot \hat{\mathbf{n}} \text{ on } \delta V \quad (10)$$

so the problem has become two dimensional. Mathematically, one can view this as solving a differential equation on a two dimensional domain, where in fact the object of investigation is still three dimensional. In the rest of this report, these two dimensional domains will be referred to as the rectangle and the two dimensional trapezoid.

2.3 Properties of internal waves

Internal waves have properties that are very different from those of normal surface waves. In this section some of these properties will be briefly touched. For a more extensive description of internal waves LeBlond & Mysak (1978) can be recommended.

One property of internal waves is that the angle of propagation of an internal wave only depends on it's frequency. The dispersion relation relates the frequency ω and the wavevector $\mathbf{k} = (k_1, k_2, k_3)$. If one assumes the solution to be a plane wave, then $p = p_0 e^{i(\mathbf{k}\mathbf{x} - \omega t)} = p_0 e^{i(k_1 x + k_2 y + k_3 z - \omega t)}$. Putting this solution in the differential equation results in :

$$k_1^2 + k_2^2 - \lambda k_3^2 = 0 \quad (11)$$

and by rearranging the terms the dispersion relation is found :

$$\omega^2 = \frac{(k_1^2 + k_2^2)N^2 + k_3^2 f^2}{k_1^2 + k_2^2 + k_3^2} \quad (12)$$

With polar coordinates the wavevector can be written as : $\mathbf{k} = \kappa(\cos(\theta)\sin(\psi), \sin(\theta)\sin(\psi), \cos(\psi))$. Here θ is the angle between $\mathbf{k}_h = (k_1, k_2, 0)$ (the projection of \mathbf{k} on the horizontal plane) and the x-axis, and ψ is the angle between k and the z-axis. In terms of \mathbf{k} itself : $\tan(\theta) = k_2/k_1$ and $\tan(\psi) = k_3/k_h$. With this notation the dispersion relation becomes :

$$\omega^2 = N^2 \sin^2(\psi) + f^2 \cos^2(\psi) \quad (13)$$

which shows that the angle ψ of the internal wave with the z-axis is only determined by it's frequency ω . Of special interest are the cases $f = 0$ and $N = 0$. When $f = 0$, the resulting waves are called internal gravity waves and when $N = 0$, they are called inertial waves.

Internal gravity waves can be found in (uniformly) stratified fluids, where gravity generates density-differences in the vertical direction. Gravity works as the restoring force. Possible frequencies for internal gravity waves are $\omega < N$. The dispersion relation is $\omega^2/N^2 = \sin^2(\psi)$ with ψ the angle between \mathbf{k} and the horizontal plane.

Inertial waves can be found in rotating homogeneous fluids. Because of the rotation pressure-differences are generated in the radial direction. The coriolis force then works as a restoring force. Possible frequencies of the inertial waves are $\omega < f$, with $f/2$ the angular velocity of the fluid. The dispersion relation is now given by : $\omega^2/f^2 = \cos^2(\psi)$.

Another important property is that for internal waves the energy propagates normal to the phase vector. The wavevector \mathbf{k} determines the direction in which single waves move. Perpendicular to the wavevector \mathbf{k} are the velocity vector \mathbf{u} of the water particles, and the group velocity vector \mathbf{c}_g which determines the direction of the energy propagation \mathbf{k} ($\mathbf{c}_g, \mathbf{u} \perp \mathbf{k}$). In figure 2 the lines on which the wavevector and the group velocity vector lie are shown. Important is that the characteristics have the same slope as the group velocity vectors. The group velocity vector can be directed in two ways. Because the energy is being transported by the water particles, \mathbf{u} and \mathbf{c}_g lie in the same plane.

The water particles move in the plane that lies perpendicular to the direction of the waves. If there is some rotation, the particles will move in elliptic orbits. If there is no rotation, so if $f = 0$, then the elliptic orbits degenerate into lines, which are parallel to \mathbf{c}_g . The group velocity is an averaged quantity and is defined by $\mathbf{c}_g = -\nabla_k \omega$. Using the dispersion relation, this can be written as :

$$\mathbf{c}_g = \frac{N^2 - \omega^2}{\omega k^2} (k_1, k_2, -\lambda k_3) \quad (14)$$

or also as :

$$\mathbf{c}_g = \frac{(N^2 - f^2)k_3^2}{k^3(N^2 k_h^2 + f^2 k_3^2)^{1/2}} (k_1, k_2, -\frac{k_h^2}{k_3^2} k_3) \quad (15)$$

If we have a wave with wavenumber $\mathbf{k} = \kappa(\cos(\theta)\sin(\psi), \sin(\theta)\sin(\psi), \cos(\psi))$ then the energy vector can be written as $\mathbf{c}_g = \hat{k}(\cos(\theta)\cos(\psi), \sin(\theta)\cos(\psi), -\sin(\psi))$. So the group velocity vector

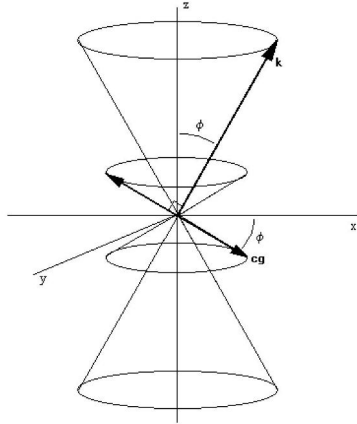


Figure 2: The vectors \mathbf{k} and \mathbf{c}_g are perpendicular and both lie on cones. The characteristic surfaces of the differential equation equal the cone formed by the \mathbf{c}_g rays. In this picture $\theta = 0$.

has the same angle θ in the horizontal plane as \mathbf{k} , but makes an angle ψ with the horizontal plane instead of the z -axis. So for each frequency, the angle of propagation for the energy is ψ , where ψ is given by the dispersion relation. ψ also happens to be the angle that the characteristic surfaces of the differential equation make with the horizontal plane, which shows that the energy is transported along the characteristics.

The manner of reflecting at boundary's is also an important property of internal waves. If an internal wave hits a sloping boundary, several things may happen. When the incoming wave lies in the plane normal to the boundary, the wave will be reflected in either the horizontal axis or the vertical axis. Which happens depends on the angle α of the boundary and on the angle ψ of the wave. When $\alpha > \psi$ the wave is reflected in the vertical axis. This is called a subcritical reflection and the slope is now steeper than the characteristics. When $\alpha < \psi$ it is reflected in the horizontal axis. This is called a supercritical reflection and the characteristics are now steeper than the slope. If the incoming wave does not lie in the plane normal to the boundary, the wave will also refract. This means that the angle θ the reflected wave will be different from that of the incoming wave. Also it's amplitude, phase and the size of it's wavenumber may be different. At vertical and horizontal boundaries, the wavenumber and the amplitude will remain equal in size, but at horizontal boundaries, the wave will be shifted in phase by 180 degrees. Since the energy movement and also the particle movement is perpendicular to the wavevector, it is more natural to look at reflections of the group velocity vector than at reflections of the wavevector. The behavior of the energy at reflection is much like that of the waves. The difference is that since $\mathbf{k} \perp \mathbf{c}_g$, if \mathbf{k} reflects in a subcritical way, then \mathbf{c}_g reflects in a supercritical way and vice versa. Also, since no energy can leave the domain through the boundary, the \mathbf{c}_g is always pointing into the domain, while \mathbf{k} can

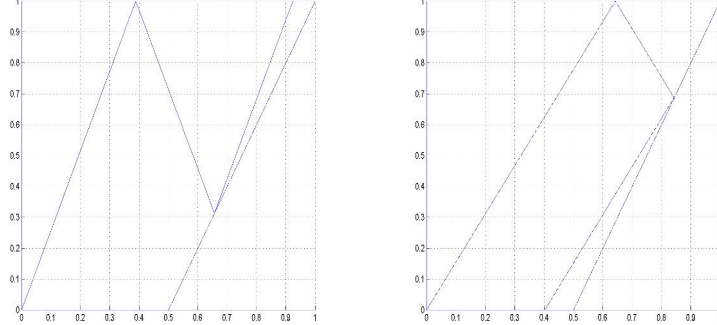


Figure 3: Two dimensional reflections of c_g in a container with a slope. The rays start in the origin and when they reach the sloping wall reflect either in the horizontal or in the vertical axis. The first picture shows a subcritical reflection ($\alpha < \psi$) and the second picture shows a supercritical reflection $\alpha > \psi$.

also point outwards. The behavior of the energy vector at the boundary is shown in figure 3.

2.4 Known solutions

Several (non numerical) solutions are known for the problem (7),(8) or a simplification of it. For internal gravity waves the problem can be analytically solved for a cube. Also for two dimensional geometry's, were a constant pressure in the perpendicular direction is assumed, the problem can be solved also analytically. For inertial waves the problem has been solved for a cube. These solutions will be discussed below in some more detail.

If the geometry is a cube, the differential equation can be solved analytically for internal gravity waves ($f = 0$). A plane wave $p(x, y, z) = \Pi e^{i(k_1 x + k_2 y + k_3 z - \omega t)}$ (so $\mathbf{u} = \mathbf{U} e^{i(k_1 x + k_2 y + k_3 z - \omega t)}$) can be assumed. Putting this in the differential equation gives the condition under which the plane wave is a solution of the differential equation : $\lambda = -\frac{k_1^2 + k_2^2}{k_3^2}$. In order to satisfy the boundary conditions the real parts of p must be taken, so $p(x, y, z) = \cos(k_1 x + k_2 y + k_3 z - \omega t)$ is a solution. This type of solution is called a global resonance. The possible wavenumbers depend on the size of the cube. If the cube is of a size $L_x \times L_y \times L_z$ then the wavenumbers are given by $(k_1, k_2, k_3) = (j_1 \pi / L_x, j_2 \pi / L_y, j_3 \pi / L_z)$ with j_1, j_2, j_3 integers. The spectrum consisting of all the possible λ 's consists of rational numbers and extends from $-\infty$ to 0. The spectrum of λ' extends from -1 to 0. There are two independent degeneracy's in the solutions space. First, if a wave (k_1, k_2, k_3) solves the differential equation, then $C(k_1, k_2, k_3)$ for arbitrary integer C is also a solution, which leaves the eigenfrequency unchanged. Also, if the aspect ratio is $\frac{L_y}{L_x} = \frac{q}{p}$, with p and q coprime, then another degeneracy exists. If a wave (k_1, k_2, k_3) is now a solution, then $(p^2 k_2, q^2 k_1, pq k_3)$ is also a solution, which again leaves the eigenfrequency unchanged. The degeneracies in

the solution space mean that for certain frequency's, there are an infinite number of solutions. This degeneracy in the solution space, which also exists for other geometry's than the cube and maybe also for three dimensional domains, can be seen as freedom in specifying the solution. For the rectangle, there is only one type of degeneracy whilst for the cube there are two types, as shown above. The general solution for the rectangle can be expressed as a fourier series :

$$p(x, z) = \sum_{j=1}^{\infty} a_j \cos(jk_1 x) \cos(jk_3 z) \quad (16)$$

One can show that by specifying the pressure as $p(x,z)=f(x,z)$ on a part of the boundary the pressure on the whole domain can be uniquely determined. The smallest interval to do so is called the fundamental interval. This fundamental interval depends on the slope of the characteristics, which in turn depends directly on the frequency of the waves. The fundamental interval also depends on the shape of the domain. Finding the fundamental interval is a matter of tracing the characteristics, where as a starting point usually a corner is taken. In figure () some fundamental intervals are shown. The factors a_j in the fourier expansion are equal to the fourier components of $f(x, z)$ over the fundamental interval. This approach using fundamental intervals can be applied to more general two dimensional domain, as described in the next paragraph. In three dimensions however, it does no longer apply readily . The reason for this is that there may be more waves that solve the differential equation, but which are not multiples (in wavenumber) of each other. One would expect however that the solution does depend only on these waves. On their own these waves give global resonance type of solutions, which can have a two dimensional or a three dimensional character. As an example for the cube with sides one, possible solutions of frequency $\omega/N = 2^{-1/2}$ are : $(k_1, k_2, k_3) = (0, 1, 1), 1, 1, 2^{1/2}$ and $(3, 4, 5)$. These solutions can be combined to form other solutions. For three dimensional solutions the relation $k_1^2 + k_2^2 = k_3^2$ has to hold for integer k_1, k_2 and k_3 .

Figure() fund.interval cube+trap+th.sol.2d.int.grav.wav.leo+pic.nature.leo?

For internal gravity waves in a container, where the geometry does not change in one, say the y-, direction, one can assume a constant pressure in this direction. So one could see this as looking at a two dimensional slice of the container. Because of this assumption, the problem (7),(8) also becomes two dimensional, because the y-derivatives drop out. The problem is now reduced to (9),(10). It has been shown by Maas & Lam (1995), that there is an algorithmic way of solving this two dimensional problem. In short, the solution can be found by tracing the characteristics as they move through the domain. By prescribing the pressure on a part of the boundary called the fundamental interval, an unique solution in terms of the pressure can be found. Along the path of each characteristic, a quantity called the partial pressure is conserved. This partial pressure corresponds to some pressure value on the fundamental interval. The pressure at any point in the domain can now be calculated by adding the partial-pressure values of the two rays that go through that point. By subtracting the partial pressure values one can find the stream function. By using this method solutions for internal gravity waves in two dimensional containers can be found.

For the two dimensional trapezoid, the spectrum consists of attractors (regions) and global resonance's (points), where the global resonance's are separated from the attractors by regions of small scale attractors. One attractor is shown in figure 5 (leo fig th?). Attractors are solutions that have fractal like properties. When there is a symmetry breaking in the domain, like the sloping boundary for the two dimensional trapezoid, focussing occurs. The sloping wall acts as a lens, which causes the energy to accumulate near a single orbit. This is a result of the symmetry breaking in combination with the reflection laws for internal waves, which do not follow snells law. In two dimensions, for attractors the energy reflects in the vertical axis at the sloping boundary. Now if some pressure distribution is taken on the fundamental interval, the focussing of rays causes a replication of this distribution on adjacent parts of the boundary, which are smaller as the attractor is approached. This self reproducing aspect is of course not limited to the boundary, but is visible in the whole domain, since the partial pressure, which equals the pressure itself on the fundamental interval is conserved on the characteristics.

When tracing along the characteristics, one is following the energy through the domain, since the \mathbf{c}_g rays run along the characteristics. Following the energy rays has also been done in three dimensions, and the results of this are in chapter 3.

For inertial waves in a cube, solutions have been found by (Maas,2001). For inertial waves in a cube one can assume a $e^{i(k_3z - \omega t)}$ dependency. To satisfy the boundary conditions at the top and the bottom again the real part of this must be taken. The resulting pressure distribution will be complex, which means that the pressure does not only oscillate in amplitude but that the pattern will also move through the domain. Since a time dependence of $e^{i\omega t}$ was assumed, the pressure can be written as : $p = (Re(p) + Im(p))e^{i\omega t} = (Re(p)\cos(\omega t) - Im(p)\sin(\omega t)) + i(Re(p)\sin(\omega t) + Im(p)\cos(\omega t))$. These solutions show amphidromic structures (pictures?). The solutions have the property that their maximum elevation is not reached at the boundary of the domain but inside the domain.

2.5 Warp

Warp is the implementation of the FEM model created by A.N.Swart. It was programmed in MATLAB, and requires the triangularisation package QMG, which also works in MATLAB. Warp is equipped with a graphical user interface (GUI), in which all of the possibilities are incorporated. Figure 4 shows a picture of the GUI.

In the top right part marked Geometry, the geometry can be entered. One can either use the Internal mesh generator for creating structured meshes of rectangular geometry's, or QMG for creating unstructured meshes of arbitrary geometry's. By using the internal mesh generator, a rectangular geometry is taken. If the QMG mesh generator is used, one can use the 'Width', 'Height' and 'Offset' for easily entering a trapezoid geometry. Also, by using QMG, one can enter more complex geometry's by using the 'Draw 2D geometry' possibility. The generated geometry's can be saved and loaded. After a geometry has been entered, by pressing 'triangulate' a triangularisation is performed on that geometry. After the triangularisation the program is ready for calculat-

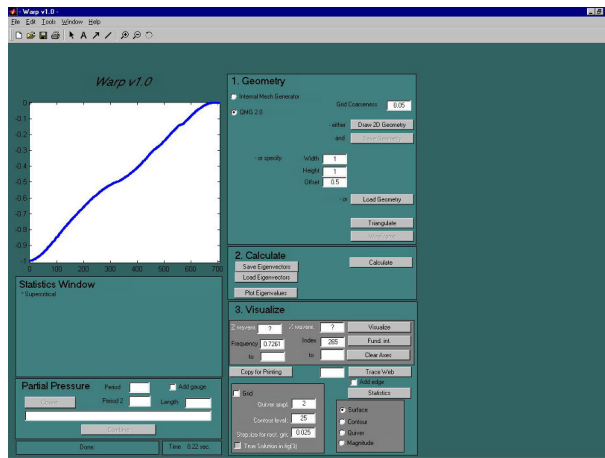


Figure 4: The graphical user interface of warp.

ing the solutions. In the middle right block marked Calculate, by pressing the button, the solutions are calculated by solving a generalized eigenvalue problem. These solutions can also be saved and loaded. To examine the eigenvalues and the corresponding eigenvectors some visualisation possibilities have been incorporated. One can see what eigenvalues have been found by pressing 'Plot eigenvalues'. In the bottom right block marked Visualize, the visualization of the solutions is controlled. By entering a index (this is the eigenvalue number), or an angle/frequency, a corresponding eigenvector can be selected for visualization. Pressing 'visualize' shows the eigenvector. By selecting one of the four possible plot options, surface plot, contour plot, velocity field or magnitude plot, the solution can be examined.

The window in the top left part is for visualization. In the picture the eigenvalues are shown of the indicated case. The options in the bottom left part marked Partial pressure are for combining solutions. The Statistics block gives some statistics.

To illustrate the workings of warp one solution is discussed. The (1,1) attractor shown in picture 5 was found at $\omega/N = 0.7477$. It was calculated using QMG and parameters coarse=0.05, height=1, width=1, offset=0.5. The surface and the contour plots show the pressure distribution. This is an attractor found by the program itself. The quiver plot shows the velocity profile and one can recognize that the velocity follows the attractor. Finally, the magnitude plot shows the size of the velocity. The high velocity magnitude near the wall is a numerical effect. One can however still clearly see the higher velocities along the attractor.

The attractor that was found does not show very much smaller structure. One reason for this is that the pressure on the fundamental interval has not been specified nicely. Warp is able to combine solutions on the basis of an interval of eigenvectors and a pressure distribution on the fundamental interval. Combining the solutions can be done by looking first at the eigenvalues. If one compares the eigenvalues that are calculated when using an unstructured grid with those calculated when using a structured grid, there seems to be a slight shift in the values. When using a structured grid, multiplicities of eigenvalues are

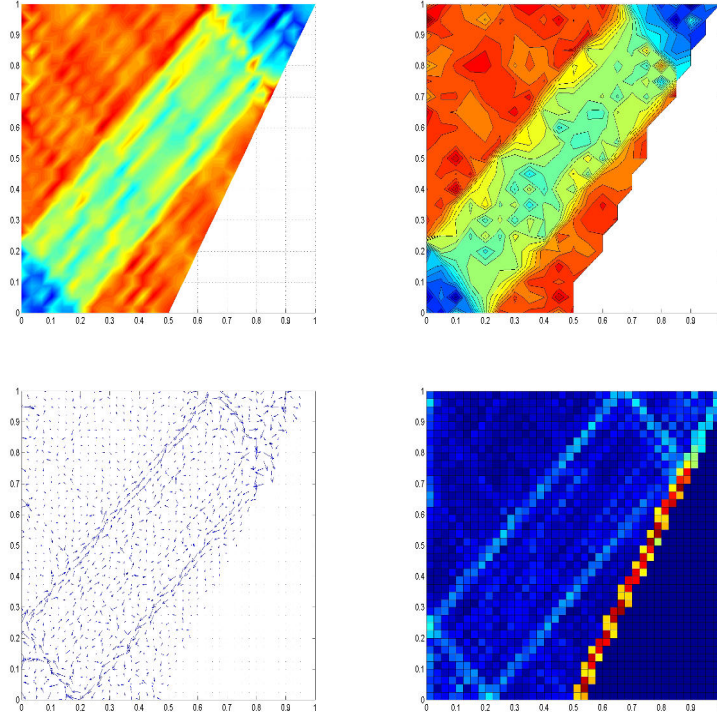


Figure 5: The different plotting possibilities of warp. From top left to bottom right are plotted : The pressure in a surface plot, the pressure in a contour plot, the velocity field in a quiver plot and the velocity field in a magnitude plot. This attractor was found using a coarseness of 0.05 at index 265.

clear, but when using an unstructured grid, this is no longer the case. When using an unstructured grid, by looking at the spectrum one can try to find groups of eigenvalues which are close to each other and combine these. Now the maximum number of eigenvectors that can be combined depends on the frequency of the internal waves. Using the fundamental interval button, this number can be checked. This combining of solutions is a discrete equivalent of the prescribing of the pressure on the fundamental interval when using the algorithmic way of solving the problem. There is a nice interpretation in terms of fourier expansions, where in this discrete case, only some lower order terms matter.

3 Analytical methods

3.1 Introduction

In this chapter a more analytical approach is taken to the problem by looking more closely to way the energy moves through the domain, and how it reflects

at the walls. The energy of the internal waves propagates along straight lines in the direction of \mathbf{c}_g . These lines, which will be referred to as rays, can be traced through the through the container. The importance of the rays lies in the fact that they shows what type of behavior is present. So global resonances and attractors can be recognized. For the 2D trapezoid and some other geometry's it is known how these rays behave. For internal gravity waves in a 2D trapezoid, a solution in terms of the pressure can even be found on the basis of the rays. It is not obvious however, how the rays will behave if they have a y-component. In section 3.2 the reflection expressions are examined. In section 3.3 the raytracing method is discussed, including the results obtained by raytracing.

3.2 Reflection expressions

Since no energy can leave the domain through the boundary, when a incoming ray $\mathbf{c}_{g,i}$ reflects from the boundary as $\mathbf{c}_{g,r}$, the sum of the normal components must vanish, so : $\mathbf{c}_{g,i} \cdot \hat{\mathbf{n}} = -\mathbf{c}_{g,r} \cdot \hat{\mathbf{n}}$. If the boundary has some slope and is given by $z = ax + C$, then this condition becomes : $-ac_{g,i,1} + c_{g,i,3} = -(-ac_{g,r,1} + c_{g,r,3})$, Using that $R^2 = \frac{c_{g,i,1}^2 + c_{g,i,1}^2}{c_{g,i,3}^2} = \frac{c_{g,r,1}^2 + c_{g,r,1}^2}{c_{g,r,3}^2} = 1/\tan(\psi)^2$, one can derive the components of the reflected ray as:

$$c_{g,r,1} = \frac{(1 + (aR)^2)c_{g,i,1} - 2aR^2c_{g,i,3}}{(1 - (aR)^2)} \quad (17)$$

$$c_{g,r,2} = c_{g,i,2} \quad (18)$$

$$c_{g,r,3} = -\frac{(1 + (aR)^2)c_{g,i,3} - 2ac_{g,i,1}}{(1 - (aR)^2)} \quad (19)$$

The formulas are very similar to the reflection expressions for the waves, as given in (Leblond). One can check that if \mathbf{k} is perpendicular to $\mathbf{c}_{g,i}$, that \mathbf{l} is then also perpendicular to $\mathbf{c}_{g,i}$ (as is expected). The way the rays behave at a sloping boundary is shown in figure 6.

In two dimensions the reflection expressions simplify to :

$$c_{g,r,1} = \frac{(1 + (aR)^2)c_{g,i,1} - 2aR^2c_{g,i,3}}{(1 - (aR)^2)} \quad (20)$$

$$c_{g,r,3} = -\frac{(1 + (aR)^2)c_{g,i,3} - 2ac_{g,i,1}}{(1 - (aR)^2)} \quad (21)$$

What happens in 2D is that when a \mathbf{c}_g ray hits the slope, it is reflected in either the horizontal or the vertical axis, depending on the value of aR . The case is high-frequency transmissive when $aR < 1$, which means that the angle of the \mathbf{c}_g rays is greater than that of the bottom slope (since if $aR < 1$ then $\tan(\alpha) < \tan(\psi)$ so $\alpha < \psi$). This means that rays will be reflected in the horizontal axis. The case is low-frequency transmissive when $aR > 1$, where the angle of the \mathbf{c}_g rays is smaller than that of the bottom slope. The rays are reflected in the vertical axis in this case. The dividing case is when the incoming group velocity (energy) vector has an angle equal to that of the bottom slope ($aR = 1$). Extreme cases are when the group velocity (energy)

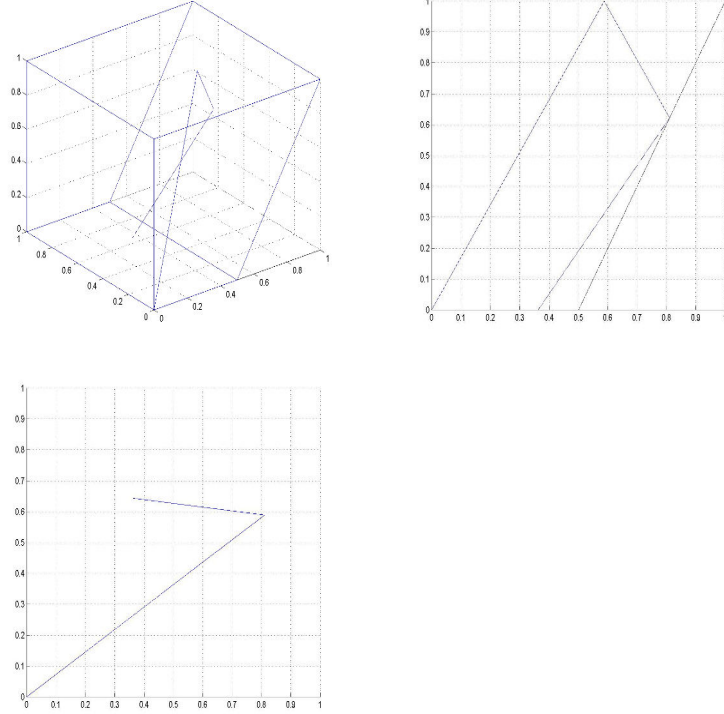


Figure 6: A reflection of a \mathbf{c}_g ray of a sloping boundary. The top left picture shows the reflection in 3d, the top right picture shows a xz projection and the bottom left picture shows a xy projection. In this last picture refracting towards the normal plane, which is here parallel to the x-axis, is visible.

vector is pointed along the slope. In the case $aR < 1$ the rays in the 2D trapezoid geometry tend to get cornered. In the case $aR > 1$ the rays can get focussed onto an attractor, fill the plane or become part of a global resonance. The rays in the 2D situation follow exactly the direction of the characteristics. In the two dimensional case, which corresponds to $k_2 = 0$ or $c_{g,2} = 0$ a ray is always reflected in either the horizontal- or the vertical axis. In the three dimensional case, this is no longer so. What happens is that when a ray hits a boundary of angle, it is refracted towards or away from the normal plane, which is the vertical plane containing $\hat{\mathbf{n}}$. Both the incoming and the outgoing rays are on the cone that has the point of reflection as it's centrepont. Depending on the value of aR , the ray is reflected up or downwards from the boundary.

Some special cases :

- Refraction : If there is a sloping boundary in the x-direction, like with the trapezoid geometry, an incoming waveray with $c_{g,i,1}=0$, so a wave that comes in parallel to the boundary, will be reflected away from the boundary, so it will get a component in de x-direction $c_{g,r,1} \neq 0$.

- reciprocity : If a ray is turned around, it will follow the same path back. So at any reflection if $\mathbf{c}_{g,i}$ is reflected as $\mathbf{c}_{g,r}$, then $-\mathbf{c}_{g,r}$ will be reflected as $-\mathbf{c}_{g,i}$.

The most important feature in the 3D case is the refraction of the rays at sloping boundaries. This allows for the energy to converge to an x-z plane, where the rays will behave just like in the 2D situation. The convergence is however very hard to predict, since convergence and divergence might both occur. So in theory, rays may never converge.

3.3 Raytrace

To see how the \mathbf{c}_g rays behave in a three dimensional domain, a raytracing program was written. The program shows that in 3d, the 2d behavior remains important. Rays which converge to attractors in the 2d case, and which are given an additional component in the y-direction, often converge to an xz plane, where the 2d case remains. Rays which converge to the corner in 2d tend to do the same thing in 3d. The raytracing program was used to do some simulations for the cube and the trapezoid.

In two dimensions the possible solutions were found :

- Attractors. If the geometry is not entirely symmetric, like in the case of the trapezoid or the tilted cube, focussing can occur. When two parallel rays reflect of a sloping boundary, they may either focus or defocus. In the case of focussing, their mutual distance will decrease, and in the case of defocussing their mutual distance will increase. If the focussing effect dominates, then the rays will approach to a single orbit, which is called the attractor. Attractors are therefor characterized as being high energy orbits. In the case of the 2D trapezoid ,when the rays are steeper then the slope, the rays will converge to the cornerpoint.
- Global resonances. If the focussing effect is exactly matched by the defocussing effect, there is a global resonance. This means that every ray will return to it's initial position in a finite number of reflections. These global resonances correspond to the eigenmodes. In order for global resonances to be possible, the geometry must have some symmetry.
- Plainfilling solutions. In this case the focussing effect is also exactly matched by the defocussing effect, but the rays will not return to their initial positions. Instead the rays reach every point in the domain.

These solutions for two dimensions were already known. Compare plots with (Maas, Nature picture). There $\tau = (1/|\tan(\psi)|)(D/L)$. In the present case : $D = 1$, $L = 1/2$ and $d = 0$, so $\tau = 2/|\tan(\psi)|$. More interesting at this point is the three dimensional behavior of the rays.

For the cube, global resonances as well as volumefilling- and plane-filling raypatterns can be expected. For the cube these different behaviors are not hard to find analytically. Global resonances can be found when $\mathbf{c}_g = \epsilon(k, l, m)$, where k, l and m are integers, and ϵ an arbitrary constant. The raypattern

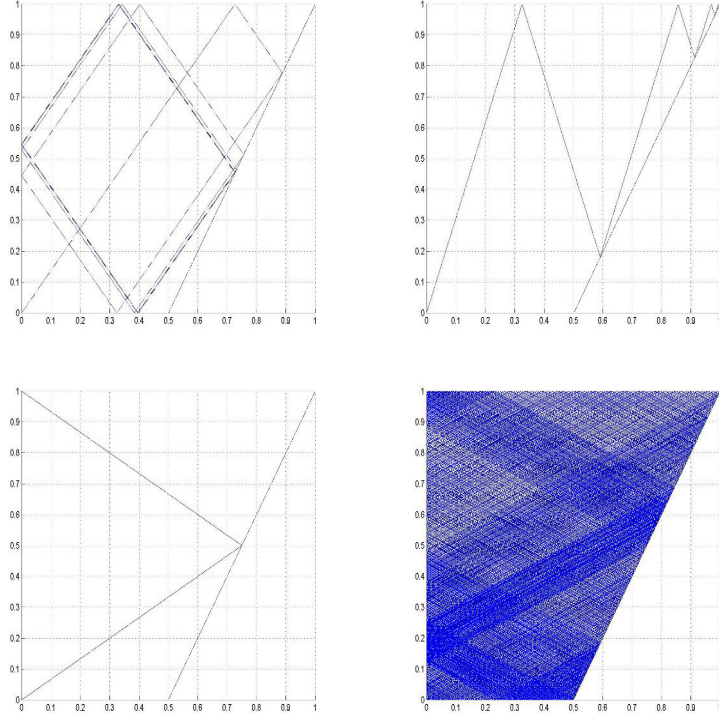


Figure 7: The different behaviors in two dimensions. Shown are from the top left to the bottom right : A line attractor, a point (cornered) attractor, a global resonance and a plane-filling solution.

reduces to a two dimensional global resonance when \mathbf{c}_g can be written in a similar form, but with a maximum of two integers. The rays become plane-filling in the direction which is left. The rays will fill the plane in all the other cases. These solutions are illustrated in figure 8.

For the trapezoid, the behavior of the rays is much more complex. Figure 9 shows the dependence of the behavior on the starting angle of the rays, when fired from one of the corners of the trapezoid. What is striking is that the two dimensional behavior remains very important.

The attractors are easy to identify. They can only occur when there is an attractor in the two dimensional situation, so for $\theta = 0$. The reason for this is that there can be no convergence only in the y -direction. When there is convergence in the x - z plane, there also must be a convergence in the y -direction because of the refraction. So other types of attractors than the ones known for the two dimensional situation are not expected. Some attractors are shown in figure 10. For almost all of the values of ψ , the attractor is eventually reached at some y -position. The number of iterations needed to

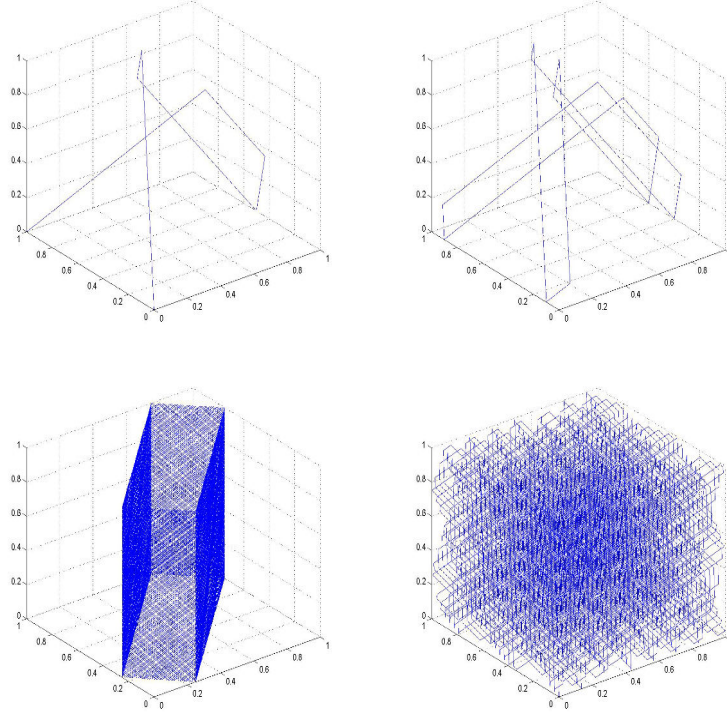


Figure 8: The different behaviors in three dimensions for the cube. From top left to bottom right a $(2,3,4)$ global resonance, the same resonance with a different starting position, a $(1,1,0)$ global resonance ($c_{g,1} = c_{g,2} = 1$ are integers and $c_{g,3} = 2^{1/2}$ is not) and a volume filling mode are shown.

converge close enough to the attractor does depend on the angle θ . When θ is small, convergence is fast, but the higher θ becomes, the more iterations are needed to converge. This can clearly be seen in picture 9. Also, for higher order attractors, the convergence is generally slower than for lower order attractors. Finally, the convergence itself is not dependent on the starting position and direction of the rays, but the speed of convergence is somewhat influenced by this.

For the trapezoid, the global resonances are not very easy to find analytically. On the basis of what is known from the behavior in the two dimensional trapezoid, one would expect global resonances to be possible in between the area's where the attractors are found. Using the pictures from the simulations, one can get a good idea where the resonances could be. Some resonances were found, and some are shown in figure 11. There seem to be no global resonances possible, for some angles however there is a kind of partial resonance. Here the resonance depends on the starting position, for some values the rays there is a resonance for others there is not. Since these resonances are however very dependent on the angles θ and ψ , and also somewhat to the starting position,

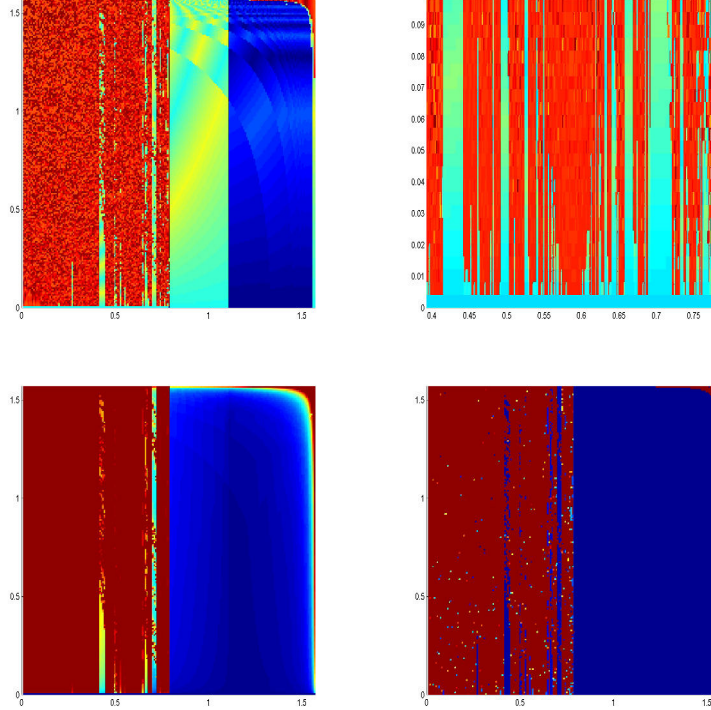


Figure 9: The dependence of the behavior of the rays in three dimensions on the angles θ and ψ . The top left picture shows the area's of convergence to two dimensions, where a difference in color indicates a difference in behavior, no convergence, a line attractor or a point attractor. The top right picture is an enlarged region of the first picture, showing the positions of higher order attractors. The bottom left picture gives an indication of the speed of the convergence. Finally, the bottom right picture shows the length of possible orbits, which gives an indication of the positions of resonances.

these resonances must be seen as rare solutions.

4 Numerical methods

4.1 Introduction

In two dimensions the behavior of the group velocity rays can be used directly to calculate the velocity and the pressure fields, where some freedom in specifying the pressure on a part of the boundary is available. In three dimensions the behavior of the group velocity rays can also be determined, as seen in chapter 3. Knowing the behavior of the rays, one can determine whether or not focussing occurs. It is not clear yet however how this information can be used to determine the three dimensional velocity and pressure fields. A way of determining what

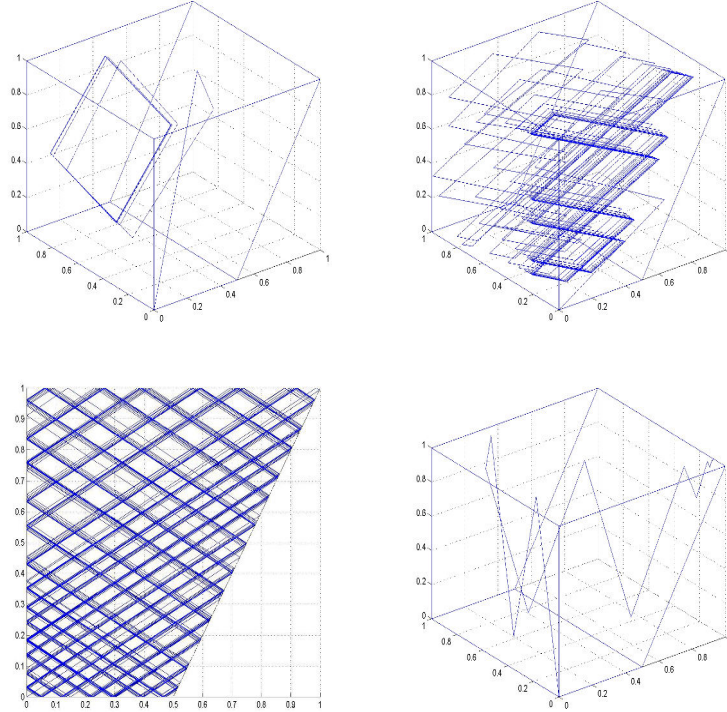


Figure 10: Attracting behavior in three dimensions. Shown are from top left to right bottom : an attractor at $\theta = 0.2\pi, \psi = 0.3\pi$, a higher order attractor at $\theta = 0.1, \psi = 0.495$, a higher order attractor at $\theta = 0.1, \psi = 0.555\pi$ (xz projection), and a point attractor at $\theta = 0.4\pi, \psi = 0.4\pi$.

kind of velocity and pressure fields might occur in three dimensions is to solve the hyperbolic differential equation describing the behavior of the internal waves in terms of the pressure. From a solution in terms of the pressure, the velocity field can be calculated. A practical way of solving the differential equation is by means of numerical approximation. To solve the differential equation, a finite element model was constructed.

In order to solve the hyperbolic differential equation, one has to resort to solving it as an eigenvalue problem. The reason for this is that there is a freedom in specifying the pressure on part of the boundary, but it is not a priori clear how much freedom there is or where one can specify dirichlet conditions. In two dimensions one can define fundamental intervals, at which the pressure can be specified and which leaves a unique solution. The size and place of the fundamental interval depends however on the frequency. In three dimensions, it is not known whether or not an equivalent of the fundamental interval can be specified. So dirichlet conditions cannot be taken, since one cannot be sure when there is overspecification. In two dimensions, the freedom in the fundamental interval is in the numerical model translated to a freedom on a finite number

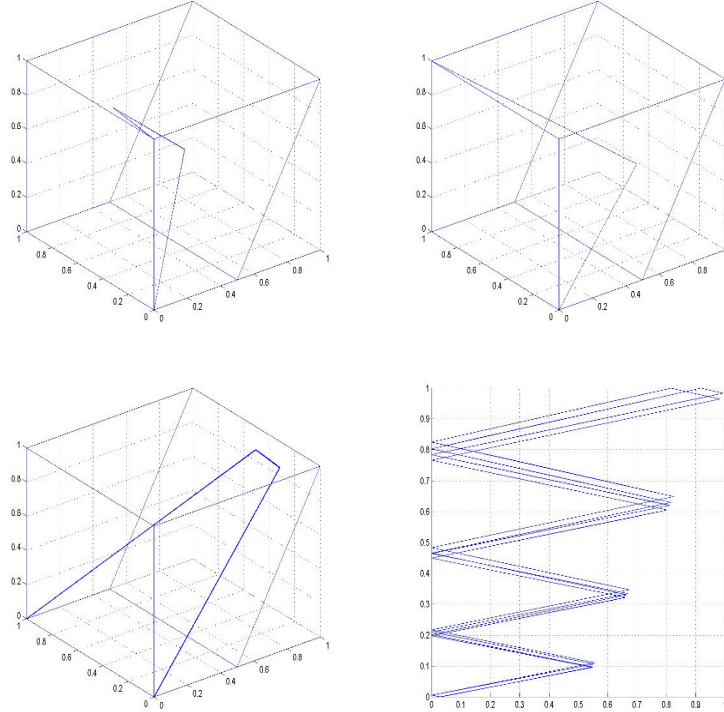


Figure 11: Shown are some resonances. These were found at the angles (θ, ψ) : $(0.7644325, 0.3851114)$, $(0.43162, 0.51167)$ and $(0.2579, 0.74035)$. For some starting positions, the resonances will disappear and make place for volume-filling modes.

of points. One can see this as a truncation of the Fourier series of the possible pressure distributions on the fundamental interval, leaving only a finite number of low order Fourier series. This is also expressed in the multiplicity of the eigenvalues. One can try to find eigenvalues that are close together and combine their eigenvectors to obtain solutions one is interested in.

In this chapter the finite element model for the three dimensional problem (7),(8) is presented. The theory is presented in section 4.2 and the implementations are presented in section 4.3.

4.2 FEM theory

Since the 3D problem does not allow for an analytical solution in the case of a trapezoid or if $f \neq 0$, it has to be handled numerically. For this purpose a finite element model was made, which was based and relies heavily upon Warp, a numerical model that was constructed for the 2D equivalent of the problem.

To solve the problem using a finite element method, one first has to find a variational formulation. To find the variational formulation one multiplies the

differential equation with a test function v and integrates over the volume V :

$$\int_V (p_{xx} + p_{yy} - \lambda p_{zz}) v \, dV = 0 \quad (22)$$

This can be rewritten as :

$$\int_V p_x v_x + p_y v_y - \lambda p_z v_z \, dV + \int_{\delta V} \frac{v}{i\omega} (\nabla p \times \mathbf{f}) \cdot \hat{\mathbf{n}} \, dO = 0 \quad (23)$$

Now by subtracting the following expressions :

$$\int_V p_{xy} v \, dV = \int_{\delta V} p_x n_y v \, dO - \int_V p_x v_y \, dV \quad (24)$$

$$\int_V p_{xy} v \, dV = \int_{\delta V} p_y n_x v \, dO - \int_V p_y v_x \, dV \quad (25)$$

and some rewriting one gets :

$$\int_V p_y v_x - p_x v_y \, dV = \int_{\delta V} (p_y, -p_x) \cdot \hat{\mathbf{n}} v \, dO = \int_{\delta V} v (\nabla p \times \mathbf{f}) \cdot \hat{\mathbf{n}} \, dO \quad (26)$$

Using this the integral can be written as $a(p, v) = 0$, where $a(p, v)$ is a (non symmetric) bilinear form :

$$a(p, v) = \int_V p_x v_x + p_y v_y - \lambda p_z v_z + \frac{f}{i\omega} (p_y v_x - p_x v_y) \, dV \quad (27)$$

The variational formulation is now : Find a $p \in \tilde{V}$ such that $a(p, v) = 0$ for $\forall v \in \tilde{V}$. For the variational space we will take $\tilde{V} = H^1(V) = W_2^1(V)$, which is the Sobolev space, defined by $W_2^1(V) = \{f \in L_{loc}^1(V) \mid \|f\|_{W_2^1(V)} < \infty\}$. This is the space of all functions f which are locally integrable, of which the first weak derivative $D_w^1 f$ exists and which have a finite sobolev norm $\|f\|_{W_2^1(V)} = (\|f\|_{L^2(V)}^2 + \|D_w^1 f\|_{L^2(V)}^2)^{1/2}$.

From the variational formulation we generate the approximation problem : Given a finite dimensional subspace $\tilde{V}_h \subset \tilde{V}$, find $p_h \in \tilde{V}_h$ such that $a(p_h, v) = 0$ for $\forall v \in \tilde{V}_h$.

The boundary conditions arise in a natural form in the variational formulation. Because there are not yet any dirichlet conditions, the solution will be unique up to an additive constant. These dirichlet conditions can be chosen later. Also since the differential equation is linear, the solutions can be combined or multiplied by constants. In the two dimensional problem, there was a clear degeneration in the set of solutions, which came from the fact that not all degrees of freedom had been used. The freedom lies in the possibility to prescribe the pressure on a part of the domain. A way to exactly use all the available degrees of freedom is by prescribing the pressure on the fundamental interval. Because of the degeneration, for some frequency's an infinite number of solutions will be possible. In the translation of the problem to an approximation of the original problem, the number of solutions for each frequency becomes

finite. In the 2D case, where one has fundamental intervals to prescribe the pressure on, one can see this as a truncation of the fourier expansion of the possible pressures on the fundamental interval.

To approximate the solution of the variational problem, a finite dimensional subspace \tilde{V}_h has to be chosen. This is done using finite elements. First the entire domain is subdivided into (open) tetraeders K_i (triangles in 2D) in such a way that the tetraeders do not overlap ($K_i \cap K_j = \emptyset$ if $i \neq j$) and that they fill the volume V ($\cup \tilde{K}_i = \tilde{V}$). Furthermore no vertex of any triangle may lie in the interior of an edge of another triangle. Such a subdivision is called a triangularisation. Using the triangularisation, finite elements (K_i, P, N) are defined on all of the subdomains K_i , where P are the shape functions and N is a basis of P' . Now $\phi_1, \phi_2, \dots, \phi_d$ is called the nodal basis and is defined by $N_i(\phi_j) = \delta_{ij}$.

The local interpolant on K_i is now given by :

$$I_{K_i} p = \sum_{i=1}^d N_i(v) \phi_i \quad (28)$$

and the global interpolant by :

$$I_T p|_{K_i} = I_{K_i} p \quad (29)$$

It is common to take for P a set of polynomials. Here for P the set of all polynomials of degree ≤ 1 , so the set of linear basisfunctions, is chosen. This means that the solution is being approximated using so called hatfunctions, which are piecewise linear functions that are unequal to zero on only a small part of the volume. Also for the nodes N , only the edges of the subdomains are chosen. To solve the approximation problem we can solve the square matrix equation $\mathbf{M} \mathbf{p}_h = 0$, where the stiffness matrix \mathbf{M} is defined with $M_{i,j} = a(\phi_i, \phi_j)$. In the variational form the frequency of the internal waves will be taken to be unknown. As a result of this, the matrix equation to be solved will be a polynomial eigenvalue problem. The order depends on the choices of f and N . If $f = 0$ is taken, so for internal gravity waves, the order is one (generalized eigenvalue problem). If $N = 0$, for inertial waves, the order is two. For $f \neq 0$ and $N \neq 0$ the order is three.

A polynomial eigenvalue problem $(\lambda^l C_l + \dots + \lambda C_1 + C_0) \mathbf{x} = 0$ can be rewritten to a generalized eigenvalue problem $\mathbf{A} \mathbf{z} = \lambda \mathbf{B} \mathbf{z}$, which is called the linearisation of the polynomial eigenvalue problem (Sleijpen (1999)). The matrices \mathbf{A} and \mathbf{B} are defined as :

$$\mathbf{A} = \begin{pmatrix} 0 & I & 0 & \dots & 0 \\ 0 & 0 & I & \dots & 0 \\ \dots & \dots & \dots & \dots & \dots \\ -C_0 & -C_1 & -C_2 & \dots & -C_{l-1} \end{pmatrix} \quad (30)$$

$$\mathbf{B} = \begin{pmatrix} I & 0 & 0 & \dots & 0 \\ 0 & I & 0 & \dots & 0 \\ \dots & \dots & \dots & \dots & \dots \\ 0 & 0 & 0 & \dots & C_l \end{pmatrix} \quad (31)$$

and $\mathbf{z} = (1, \lambda, \dots, \lambda^{l-1})\mathbf{x}^T$.

The elements of the stiffness matrix are given by $M_{i,j} = a(\phi_i, \phi_j)$:

$$M_{i,j} = \int_V (\phi_i)_x (\phi_j)_x + (\phi_i)_y (\phi_j)_y - \lambda (\phi_i)_z (\phi_j)_z + \frac{f}{i\omega} ((\phi_i)_y (\phi_j)_x - (\phi_i)_x (\phi_j)_y) dV \quad (32)$$

This can be rewritten as :

$$\begin{aligned} M_{i,j} &= \omega^3 \int_V (\phi_i)_x (\phi_j)_x + (\phi_i)_y (\phi_j)_y + (\phi_i)_z (\phi_j)_z dV \\ &- \omega \int_V N^2 ((\phi_i)_x (\phi_j)_x + (\phi_i)_y (\phi_j)_y) + f^2 (\phi_i)_z (\phi_j)_z dV \\ &+ (\omega^2 - N^2) if \int_V (\phi_i)_y (\phi_j)_x - (\phi_i)_x (\phi_j)_y dV \end{aligned} \quad (33)$$

This is an third order polynomial eigenvalue problem. Using this general form some simplifications can easily be made. Because only linear basisfunctions are being used, all the derivatives of the basisfunctions are constants and so:

$$\begin{aligned} M_{i,j} &= (\omega^3 ((\phi_i)_x (\phi_j)_x + (\phi_i)_y (\phi_j)_y + (\phi_i)_z (\phi_j)_z) \\ &- \omega (N^2 ((\phi_i)_x (\phi_j)_x + (\phi_i)_y (\phi_j)_y) + f^2 (\phi_i)_z (\phi_j)_z) \\ &+ (\omega^2 - N^2) if ((\phi_i)_y (\phi_j)_x - (\phi_i)_x (\phi_j)_y) \int_V 1 dV \end{aligned} \quad (34)$$

The linear basisfunctions are given by :

$$\det \begin{pmatrix} x - x_1 & y - y_1 & z - z_1 & \phi_i - \phi_{i,1} \\ x_2 - x_1 & y_2 - y_1 & z_2 - z_1 & \phi_{i,2} - \phi_{i,1} \\ x_3 - x_1 & y_3 - y_1 & z_3 - z_1 & \phi_{i,3} - \phi_{i,1} \\ x_4 - x_1 & y_4 - y_1 & z_4 - z_1 & \phi_{i,4} - \phi_{i,1} \end{pmatrix} = 0 \quad (35)$$

, where $\phi_{i,j}$ is the value of the i -th basisfunction in node j (with 4 nodes in each tetraeder). This gives :

$$\phi_i = \phi_{i,1} + (1/d)(c_{i,1}(x - x_1) + c_{i,2}(y - y_1) + c_{i,3}(z - z_1)) \quad (36)$$

where :

$$d = \det \begin{pmatrix} x_2 - x_1 & y_2 - y_1 & z_2 - z_1 \\ x_3 - x_1 & y_3 - y_1 & z_3 - z_1 \\ x_4 - x_1 & y_4 - y_1 & z_4 - z_1 \end{pmatrix} \quad (37)$$

$$c_{i,1} = \det \begin{pmatrix} y_2 - y_1 & z_2 - z_1 & \phi_{i,2} - \phi_{i,1} \\ y_3 - y_1 & z_3 - z_1 & \phi_{i,3} - \phi_{i,1} \\ y_4 - y_1 & z_4 - z_1 & \phi_{i,4} - \phi_{i,1} \end{pmatrix} \quad (38)$$

$$c_{i,2} = -\det \begin{pmatrix} x_2 - x_1 & z_2 - z_1 & \phi_{i,2} - \phi_{i,1} \\ x_3 - x_1 & z_3 - z_1 & \phi_{i,3} - \phi_{i,1} \\ x_4 - x_1 & z_4 - z_1 & \phi_{i,4} - \phi_{i,1} \end{pmatrix} \quad (39)$$

$$c_{i,3} = \det \begin{pmatrix} x_2 - x_1 & y_2 - y_1 & \phi_{i,2} - \phi_{i,1} \\ x_3 - x_1 & y_3 - y_1 & \phi_{i,3} - \phi_{i,1} \\ x_4 - x_1 & y_4 - y_1 & \phi_{i,4} - \phi_{i,1} \end{pmatrix} \quad (40)$$

For each tetraeder there are four basisfunctions, which are given by ϕ_i ($\phi_{i,j} = 1$ if $i = j$ and $\phi_{i,j} = 0$ if $i \neq j$). The derivatives of the basisfunctions are now constants (bv $\phi_x = c_1/d$). Using the constant derivatives, the elements of the stiffness matrix can be computed. Filling in the derivatives gives :

$$\begin{aligned} M_{i,j} &= (1/d^2)(\omega^3(c_{i,1}c_{j,1} + c_{i,2}c_{j,2} + c_{i,3}c_{j,3}) \\ &\quad - \omega(N^2(c_{i,1}c_{j,1} + c_{i,2}c_{j,2}) + f^2c_{i,3}c_{j,3}) \\ &\quad + (\omega^2 - N^2)if(c_{i,2}c_{j,1} - c_{i,1}c_{j,2})) \int_V 1 \, dV \end{aligned} \quad (41)$$

with :

$$\int_V 1 \, dV = (1/6)\det \begin{pmatrix} x_1 & y_1 & z_1 & 1 \\ x_2 & y_2 & z_2 & 1 \\ x_3 & y_3 & z_3 & 1 \\ x_4 & y_4 & z_4 & 1 \end{pmatrix} \quad (42)$$

The calculation of the stiffness matrix is usually done using element stiffness matrices, which contain the contributions for the individual elements. Per element, the basisfunctions are linear functions, while on the whole domain, they are piecewise linear functions, hatfunctions. Using the element stiffness matrices, the stiffness matrix is then computed by summing the element contributions of $a(\phi_i, \phi_j)$ for each combination of two basisfunctions. Since most basisfunctions don't overlap, the resulting stiffness matrix will be sparse.

If one assumes a solution of the form $p = p(x, z)e^{i(k_2y - \omega t)}$ where k_2 is taken to be a constant, the problems dimension is reduced from three down to two. Using that $p_y = ik_2p$, $v = v(x, z)$ (so $v_y = 0$) in the bilinear form $a(p, v)$ a new bilinear form $\tilde{a}(p, v)$ is found :

$$\tilde{a}(p, v) = \int_V p_x v_x - \lambda p_z v_z + k_2^2 p v + \frac{f k_2}{\omega} (p v_x) \, dV \quad (43)$$

The elements of the stiffness matrix are given by $\tilde{M}_{i,j} = a(\phi_i, \phi_j)$:

$$\tilde{M}_{i,j} = \int_V (\phi_i)_x (\phi_j)_x - \lambda (\phi_i)_z (\phi_j)_z + k_2^2 \phi_i \phi_j + \frac{fk_2}{\omega} (\phi_i (\phi_j)_x) dV \quad (44)$$

This can be rewritten as :

$$\begin{aligned} \tilde{M}_{i,j} &= \omega^3 \int_V (\phi_i)_x (\phi_j)_x + (\phi_i)_z (\phi_j)_z + k_2^2 \phi_i \phi_j dV \\ &- \omega \int_V N^2 ((\phi_i)_x (\phi_j)_x + k_2^2 \phi_i \phi_j) + f^2 (\phi_i)_z (\phi_j)_z dV \\ &+ (\omega^2 - N^2) f k_2 \int_V \phi_i (\phi_j)_x dV \end{aligned} \quad (45)$$

To evaluate this expression, integrals of basisfunctions and of products of two basisfunctions must be calculated. In order to do so, it is convenient to transform the triangles (2D), to the standard triangle with edges $(x,z) : (0,0), (0,1)$ and $(1,0)$. Suppose we look at a triangle with edges $(x_1, z_1), (x_2, z_2), (x_3, z_3)$, with area O . The linear basisfunctions are given by :

$$\det \begin{pmatrix} x - x_1 & z - z_1 & \phi_i - \phi_{i,1} \\ x_2 - x_1 & z_2 - z_1 & \phi_{i,2} - \phi_{i,1} \\ x_3 - x_1 & z_3 - z_1 & \phi_{i,3} - \phi_{i,1} \end{pmatrix} = 0 \quad (46)$$

which gives :

$$\phi_i = \phi_{i,1} + (1/d)(c_{i,1}(x - x_1) + c_{i,2}(z - z_1)) \quad (47)$$

with :

$$d = (x_2 - x_1)(z_3 - z_1) - (x_3 - x_1)(z_2 - z_1) \quad (48)$$

$$c_{i,1} = (z_3 - z_1)(\phi_{i,2} - \phi_{i,1}) - (z_2 - z_1)(\phi_{i,3} - \phi_{i,1}) \quad (49)$$

$$c_{i,2} = (x_2 - x_1)(\phi_{i,3} - \phi_{i,1}) - (x_3 - x_1)(\phi_{i,2} - \phi_{i,1}) \quad (50)$$

Now define transformation f and g by :

$$x = f(\epsilon, \nu) = (x_2 - x_1)\epsilon + (x_3 - x_1)\nu + x_1 \quad (51)$$

$$z = g(\epsilon, \nu) = (z_2 - z_1)\epsilon + (z_3 - z_1)\nu + z_1 \quad (52)$$

then ϕ_i can be written as :

$$\phi_i(f(\epsilon, \nu), g(\epsilon, \nu)) = \phi_{i,1} + (1/d)(\alpha\epsilon + \beta\nu) \quad (53)$$

with :

$$\alpha = (x_2 - x_1)c_{i,1} + (z_2 - z_1)c_{i,2} \quad (54)$$

$$\beta = (x_3 - x_1)c_{i,1} + (z_3 - z_1)c_{i,2} \quad (55)$$

This gives :

$$\phi_i(f(\epsilon, \nu), g(\epsilon, \nu)) = \epsilon(\phi_{i,2} - \phi_{i,1}) + \nu(\phi_{i,3} - \phi_{i,1}) + \phi_{i,1} \quad (56)$$

and now :

$$\det \left(\begin{bmatrix} \frac{\partial}{\partial \epsilon} \mathbf{x}(\epsilon, \nu) & \frac{\partial}{\partial \nu} \mathbf{x}(\epsilon, \nu) \\ \frac{\partial}{\partial \epsilon} \mathbf{z}(\epsilon, \nu) & \frac{\partial}{\partial \nu} \mathbf{z}(\epsilon, \nu) \end{bmatrix} \right) = d \quad (57)$$

We can now calculate the two needed integrals, where the integration is done over one triangle K :

$$\int_K \phi_i \phi_j dO = \int_0^1 \int_0^{1-\epsilon} \phi_i(f(\epsilon, \nu), g(\epsilon, \nu)) \phi_j(f(\epsilon, \nu), g(\epsilon, \nu)) d\nu d\epsilon \quad (58)$$

This evaluates to $d/12$ if $i = j$ and to $d/24$ if $i \neq j$.

$$\int_K \phi_i dV = \int_0^1 \int_0^{1-\epsilon} \phi_i(f(\epsilon, \nu), g(\epsilon, \nu)) d\nu d\epsilon = d/6 \quad (59)$$

Thus, the stiffness matrix $\tilde{\mathbf{M}}$ becomes :

$$\begin{aligned} \tilde{M}_{i,j} = & \omega^3 ((c_{i,1} c_{j,1} + c_{i,2} c_{j,2}) O/d^2 + k_2^2 d \int_{T_{st}} \phi_i \phi_j dV) \\ & - \omega ((N^2 c_{i,1} c_{j,1} + f^2 c_{i,2} c_{j,2}) O/d^2 + N^2 k_2^2 d \int_{T_{st}} \phi_i \phi_j dV) \\ & + (\omega^2 - N^2) f k_2 c_{j,1} d/6 \end{aligned} \quad (60)$$

, where the integral over T_{st} , which the standard triangle, evaluates to $d/12$ if $i = j$ and to $d/24$ if $i \neq j$.

To check if amphidromic structures would be visible for inertial waves in a cube shaped container, another simplification was made. In a cube shaped container one can assume a pressure distribution of $p = p(x, y) \cos(k_3 z) e^{-i\omega t}$. Using this in (7),(8) the resulting problem becomes :

$$p_{xx} + p_{yy} + \lambda k_3^2 p = 0 \text{ on } V \quad (61)$$

$$(p_x, p_y, 0) \cdot \hat{\mathbf{n}} = -\frac{1}{i\omega} (\nabla p \times \mathbf{f}) \cdot \hat{\mathbf{n}} \text{ on } \delta V \quad (62)$$

4.3 FEM implementations

The QZ algorithm that is used by MATLAB's eig function, which can calculate all the generalized eigenvalues and eigenvectors of a $\mathbf{A}\mathbf{x} = \lambda\mathbf{B}\mathbf{x}$, is of order n^3 , where n is the size of the matrices \mathbf{A} and \mathbf{B} . So if the matrix size is doubled, the execution time will be multiplied by a factor $2^3 = 8$, for n large.

Now for solving the polynomial eigenvalue problems they can be rewritten to a generalized eigenvalue problem, but this gives a larger matrix. For a polynomial eigenvalue problem of order m , one gets a matrix size of nm . In the present problem the size n of the matrix is equal to the number of nodes used in the triangularisation. Also, the size of m depends on the type of internal waves that are examined. For internal gravity waves $m = 1$, for inertial waves $m = 2$ and for combinations of both $m = 3$. This means that computation on internal gravity waves are about 8 times faster for large n than those for inertial waves. Another aspect is that for internal gravity waves the matrix is real, but in all other cases it is complex, which also gives a higher computation time for inertial waves.

The implementations of the FEM can roughly be divided into four steps. First the mesh has to be created. Starting by defining a two or three dimensional geometry, a triangularisation is performed on the geometry. This means that the domain is divided into non-overlapping triangles or tetraeders. In the implementations, the triangularisation is performed by the program QMG. Resulting from the triangularisation are the matrices, \mathbf{Z} containing the positions of the nodes, and \mathbf{T} containing the vertices. After this, the element stiffness matrices, m in total, are calculated. These matrices contain the contributions of the different basisfunctions in each of the finite elements. These calculations are the implementations of the expressions found in the previous section. The detailed calculations are done in the function `makestiff3d`. The calculation of the element stiffness matrices is done by the functions `elmstiff` and `makestiff`. The stiffness matrices are now calculated by taking for each basisfunction the sum of the individual contributions for the relevant elements.

These stiffness matrices form the matrices of the polynomial eigenvalue problem. Using the stiffness matrices, the two matrices for the generalized eigenvalue problem are determined. This is all done by the function `assemble`. Finally, the generalized eigenvalue problem is solved by the function `eigsolve`. This results in the matrices for the generalized eigenvalues and the corresponding eigenvectors.

5 Numerical results

5.1 Introduction

In this chapter the numerical results are presented and discussed. Where possible an attempt to validate the results is made. In section 5.2 the results for internal gravity waves are discussed. In section 5.3 the results for inertial waves are discussed.

5.2 Internal gravity waves

For solving the problem when $f = 0$, so looking only at internal gravity waves, two programs were written. The first is the implementation of the FEM for solving the simplified case, when a pressure distribution in the y-direction is assumed. This program was called `warpn` (for now). The second program is the implementation of the FEM for solving the problem in the full three dimensions. This program was called `3dn`. Both programs were tested using the cube as a container, for which the exact solutions are known. Both programs were

also applied to a trapezoidal shaped container. For the trapezoid the solutions are known for those cases when the pressure doesn't vary in the y-direction. The programs were also compared with these known solutions. Finally, the programs were used to see if any other solutions for the trapezoid could be found.

First the solutions of warpn are will be discussed, and later the solutions of 3dn. In figure 12 some of the eigenvalue spectra obtained using warpn are shown. An important feature of these spectra is that for increasing k , the lower eigenvalues disappear, as can be seen in the bottom right picture for the trapezoid. This can be explained best by looking at the cube. For the cube the eigenvalues are given by $\omega/N = \frac{k_1^2 + k_2^2}{k_1^2 + k_2^2 + k_3^2}^{1/2}$. Now this expression goes to zero when $\frac{k_3^2}{k_1^2 + k_2^2}$ goes to infinity. When k_2 is large when compared to k_1 and k_2 , low eigenvalues no longer occur. Another way of looking at this is by realising that low eigenvalues are related to energy rays that make a small angle with the horizontal plane. By assuming a large k_2 value a low steepness in the y-direction is more probable.

In figure 13 some solutions of warpn are shown. For $k_2 = 0$ the normal attractors are visible. Looking at $k_2 = \pi$ an attractor like shape is still visible, but it has a three dimensional solution, since the pressure is no longer constant in the y-direction. For $k_2 = 10\pi$ the rays still suggest an attractor like solution (since this is a geometric property), but high frequency oscillations are visible in the solution, probably due to the high k_2 . Because of this the energy rays are not very steep. For example rays that have no x-component will, when out of reach of the sloping wall, reflect often at the front and back walls. Clearly visible in all the solutions are the characteristics. The high frequency oscillations were also observed a lot for the cube with $k_2 = 10\pi$.

Shown in figure 14 are some solutions found by 3dn. As could be expected, solutions with a constant pressure in the y-direction were found, for both the cube and the trapezoid. For 3dn, the distribution of the eigenvalues depends on the spacing of the grid. In figure 14, the eigenvalues correspond to a grid that is narrow in the xz plane and more coarse in the y direction. In the eigenvalues, the kind of curved structures, which are known from warp, can be recognized. In warp, these structures represented groups of eigenvalues having the same frequency. When the grid is unstructured, these eigenvalues were found to be somewhat spaced apart. Looking at the eigenvalues for 3dn, it is likely that a similar thing occurs in three dimensions. One could therefor try to combine those solutions which, on the basis of the eigenvalue plots, appear to be in the same group, and therefor may have the same frequency. (compare with structured grid eigenvalues)

5.3 Inertial waves

For solving the problem for inertial waves, so for $N = 0$, three programs were used. The first, warpf, assumes like in warpn, a wavelike solution in the y-direction, and then solves the problem which has become 2 dimensional. The second program, 3df, is like 3dn the full 3 dimensional case. The last, warpfz,

assumes a pressure distribution of $e^{i(k_3 z - \omega t)}$ in the z-direction. This spin-off program was used only for testing for the a cubeshaped container, because in this case the solutions are known. Below some result of the programs will be shown.

Amphidromic structures : cube coarse 25, rect. coarse 20.

First we will look at warpfz. When applied to a cube shaped container, the solutions are known to be amphidromic structures. In picture 15 some solutions are shown. Although this is a spin off program, the result do give some credibility to the other programs. The results were checked and found to agree with the solutions found by (Leo,ampstr). The finite element code also came up with series of alternative solutions, which did not seem to make much sense physically, but are probably a result of trying to comply to the boundary conditions in a local way.

Using warpf also some attractor like structures were found. One solution here is especially interesting. For $k = \pi$, an attractor like structure was found for $\omega/f = 0.6876$. This solution corresponds very good to one found using warpn, namely the solution at $\omega/N = 0.7535$. These two solutions happen to be at about the same angle ψ .

With 3df solutions for the full 3 dimensional problem for inertial waves can be determined.

6 Conclusions Summary

References

- BRENNER, S. C. & SCOTT, L. R. 1994 *The Mathematical Theory of Finite Element Methods*. Springer Verlag.
- YIH, C. S. 1980 *Stratified Flows*. Academic Press.
- FRIEDLANDER, S. & SIEGMAN, W. L. 1982 Internal waves in a contained rotating stratified fluid. *Journal of Fluid Mechanics* **114**, 123–156.
- GERKEMA, T. & ZIMMERMAN, J. 1999 *Interne Golven [Lecture notes, in Dutch, revised edition edn*. University of Utrecht.
- GILDING, B. H. & KUERTEN, J. G. M. 1997 *Partiele differentiaalvergelijkingen uit de mathematische fysica [Lecture notes, in dutch]*, University of Enschede.
- GREENSPAN, H. 1968 *The theory of rotating fluids..* Cambridge University Press.
- HENDERSON, G. A. & ALDRIDGE, K. D. 1992 A finite-element method for inertial waves in a frustum. *Journal of Fluid Mechanics* **234**, 317–327.
- JOHNSON, R. S. 1997 *A modern introduction to the mathematical theory of water waves*. Cambridge University Press.
- LEBLOND, P. & MYSAK, L. 1978 *Waves in the ocean*. Elsevier.

- MAAS, L. R. 2000 *On the amphidromic structure of contained inertial waves (working document)*.
- MAAS, L. R. & LAM, F.-P. A. 1995 Geometric focusing of internal waves. *Journal of Fluid Mechanics* **300**, 1–41.
- MAAS, L. R., LAM, F.-P. A., BENIELLI, D. & SOMMERIA, J. 1997 Observation of an internal wave attractor in a confined stably stratified fluid. *Nature* **388**, 557–561.
- RIEUTORD, M., DINTRANS, B. & VALDETTARO, L. 1999 Gravito-inertial waves in a rotating stratified sphere or spherical shell. *Journal of Fluid Mechanics* **398**, 271–297.
- SEWELL, G. 1985 *Analysis of a Finite Element Method: PDE/PROTRAN*. Springer Verlag.
- SLEIJPEN, G. L. G., VAN DER VORST, H. A. & BAI, Z. 1999 *Jacobi-davidson algorithms for various eigenproblems [working document]*.
- SWART, A. N. 2000 *A finite element method for internal gravity waves*. University of Utrecht.
- SWART, A. N. 2000 *The Warp User and Developer Manual*. University of Utrecht.
- TOLSTOY, I. 1973 *Wave Propagation*. McGraw-Hill.
- VAVASIS, S. M. 1999 The qmg 2.0 mesh generator <http://www.cs.cornell.edu/home/vavasis/qmg-home.html>.

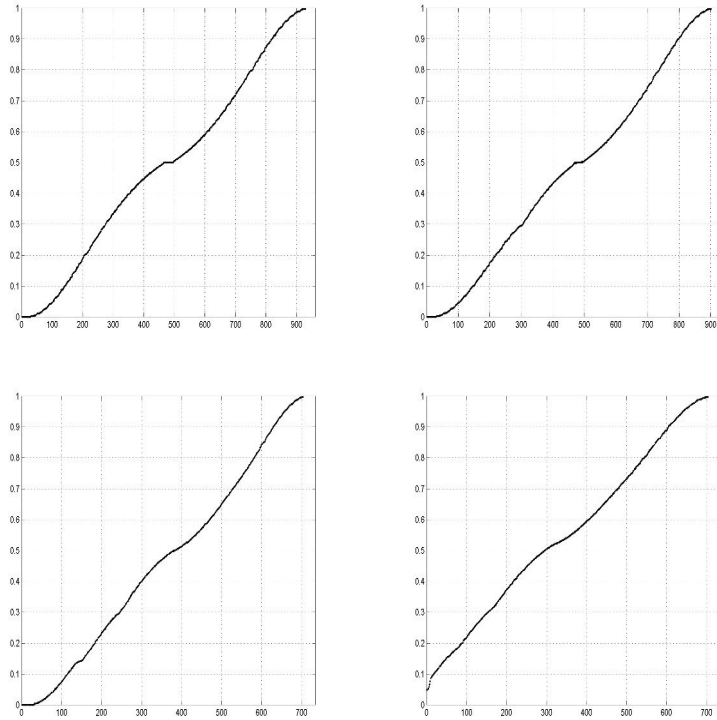


Figure 12: Some eigenvalue plots showing ω/N as a function of the ordered eigenvalue index. The top left picture shows the eigenvalues for the cube, using a structured grid ($k_2 = 0$). The multiplicities of some of the eigenvalues are clearly visible. The top right picture shows the eigenvalues for the cube using an unstructured grid ($k_2 = 0$). Comparing this plot with that of the unstructured grid, one can see that the multiplicities have spread out somewhat and are no longer exact. In the bottom left picture the eigenvalues for the trapezoid ($k_2 = 0$) are shown. There are some minor shifts, but the overall picture is comparable with the eigenvalues of the cube. Finally, in the bottom right picture the eigenvalues for the trapezoid ($k_2 = 10\pi$) are shown. Clearly visible is that the lower eigenvalues have dissapeared.

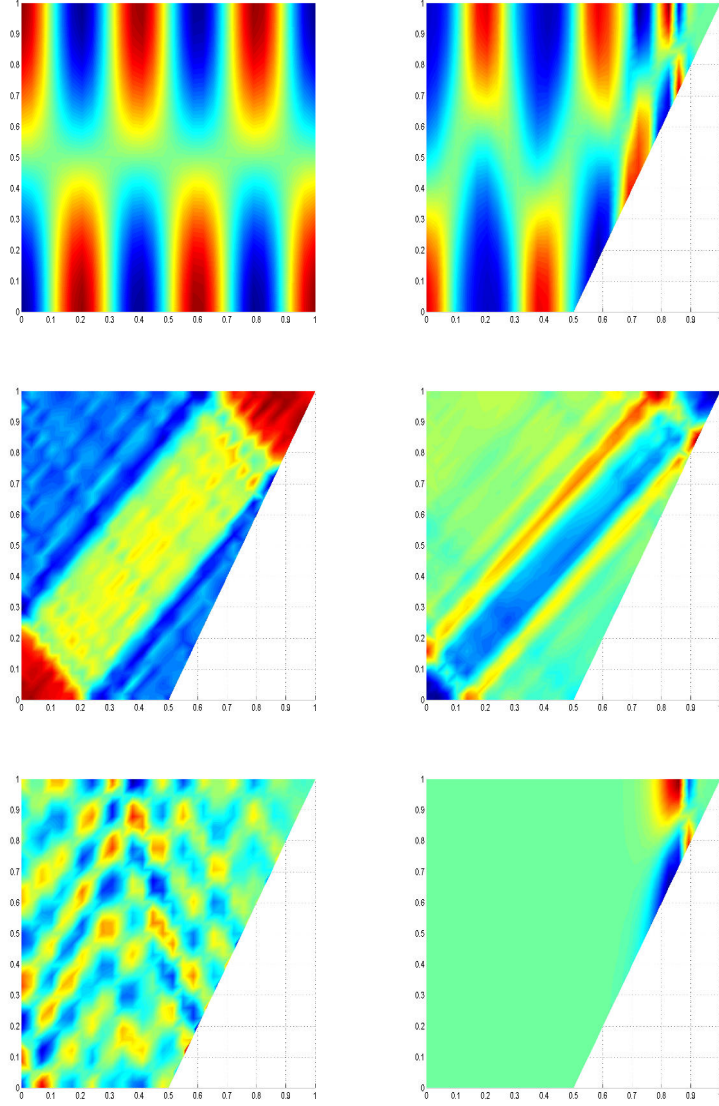


Figure 13: Shown in the pictures are some solutions obtained using warpn. The solutions show the pressure distribution. In the top left picture a (5,10,1) global resonance for the cube ($k_2 = 10\pi$) is shown. It was found at $\omega/N = 0.9958$. In theory this global resonance would be at $\omega/N = \frac{k_1^2 + k_2^2}{k_1^2 + k_2^2 + k_3^2}^{1/2} = (125/126)^{1/2} = 0.9960$. In the top right picture a point attractor is shown. In the middle left, right and bottom left picture attractor like structures for $k_2 = 0$, $k_2 = \pi$ and $k_2 = 10\pi$ are shown. In the bottom right picture another solution is shown $k_2 = 10\pi$.

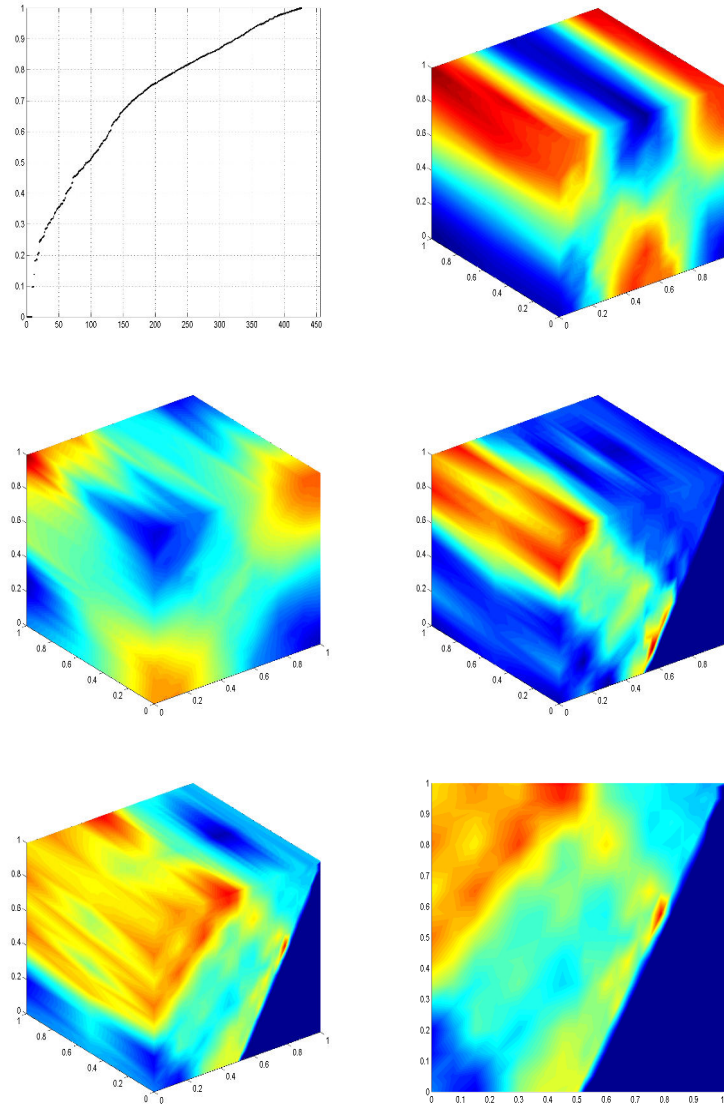


Figure 14: Some solutions of 3dn. The top left picture shows the eigenvalues ω/N ordered by their size. The top right picture and the middle left picture show global resonances for the cube for frequency's 0.8927 and 0.8019. The second of these global resonances is a (1,1,1) global resonance. In theory one would expect this resonance when $\omega/N = \frac{k_1^2+k_2^2}{k_1^2+k_2^2+k_3^2}^{1/2} = (2/3)^{1/2} = 0.8165$. The other three pictures show attractors at frequency's 0.8115 and 0.7622.

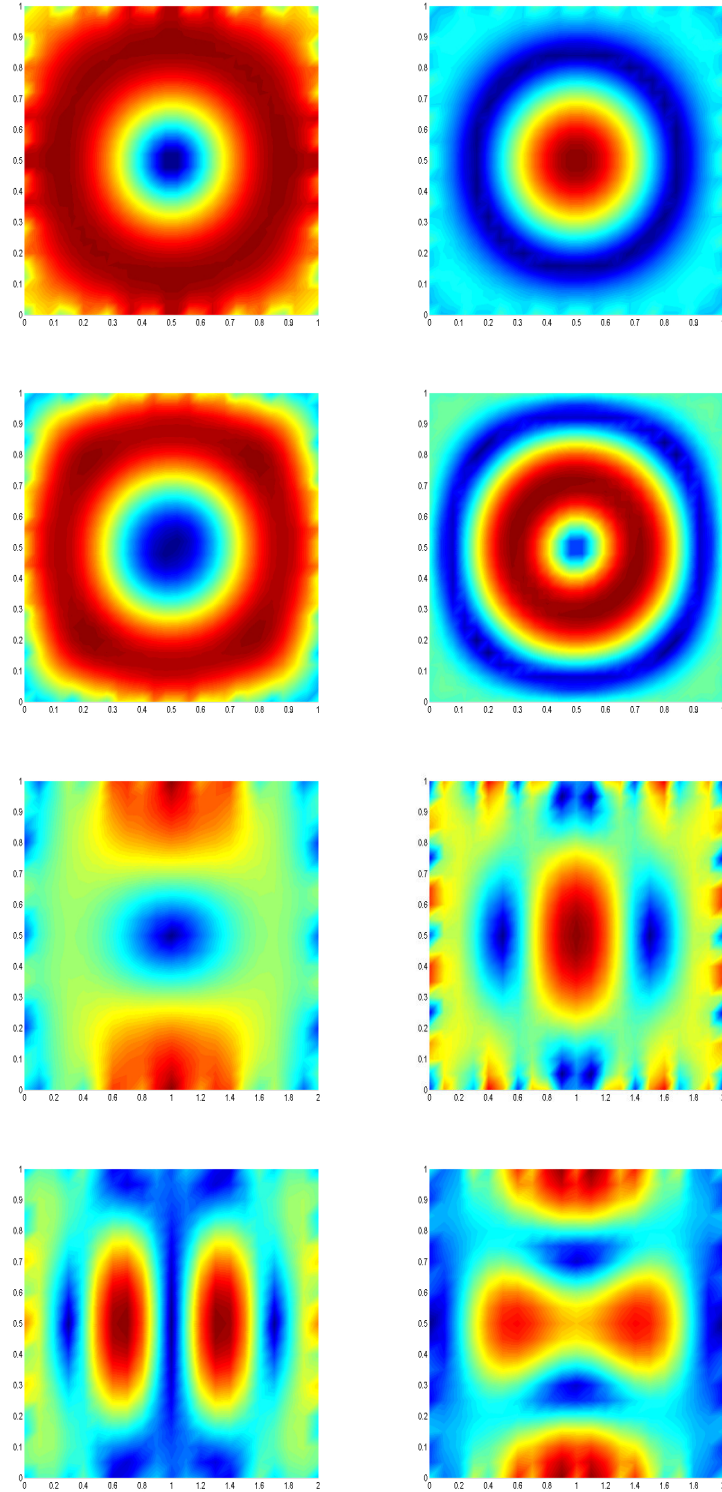


Figure 15: Amphidromic structures, as calculated using warpfz. Plotted is the pressure as $(\text{Re}(p)^2 + \text{Im}(p)^2)^{1/2}$. The top four plots are for a 1x1 rectangular container, the bottom four are for a 2x1 rectangular container. The amphidromic structures were found at frequency's ω/f : 0.5460, 0.4166, 0.3675, 0.3394 and 0.6557, 0.5621, 0.4726, 0.4303.

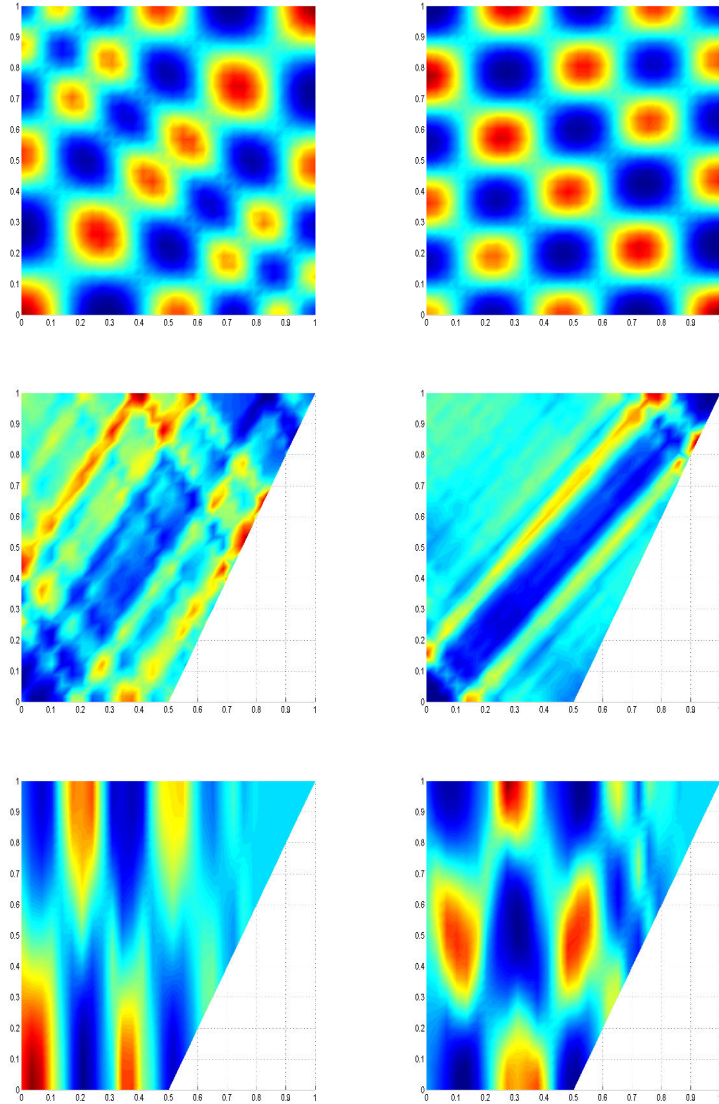


Figure 16: Shown are some solutions calculated using warpf. The pictures show the pressure distributions as $(\text{Re}(p)^2 + \text{Im}(p)^2)^{1/2}$. In the top two pictures solutions for the cube with $k_2 = \pi$ are shown. These were found at frequency's 0.6962 and 0.7686. In the middle two pictures attractor like solutions for the trapezoid with $k_2 = \pi$, found at frequency's 0.6117 and 0.6876, are shown. In the bottom two pictures two solutions for the trapezoid with $k_2 = 10\pi$, found at frequency's 0.0667 and 0.1658 are shown.

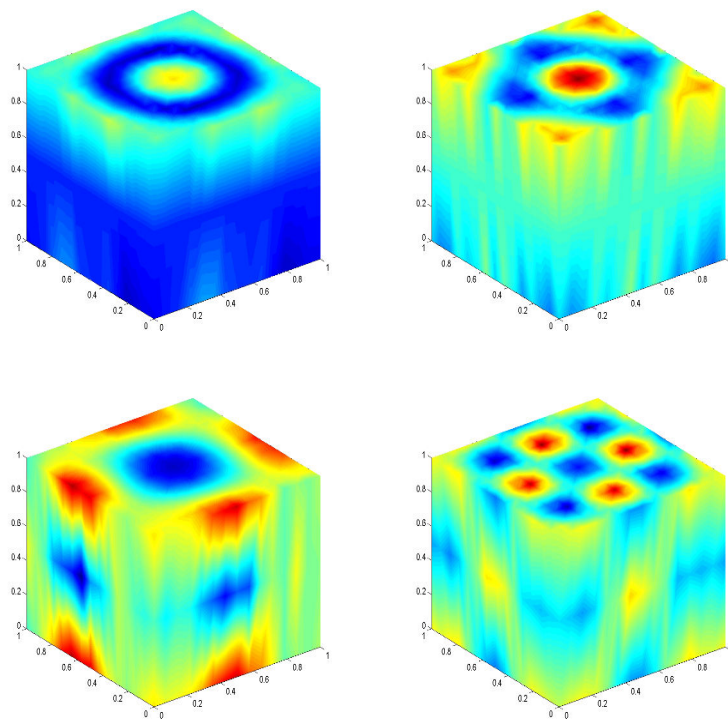


Figure 17: Shown is a solution for the cube found using 3df. Frequency's 0.3826, 0.2350 resp. 0.4875, 0.2642.